SCIENTIFIC REPORTS

OPEN

SUBJECT AREAS:
ENVIRONMENTAL BIOTECHNOLOGY
ELECTROCATALYSIS
RENEWABLE ENERGY
BIONANOELECTRONICS

Received
16 April 2013

Accepted
20 December 2013

Published
16 January 2014

Correspondence and requests for materials should be addressed to H.-Q.Y. (hqyu@ustc.edu.cn)

* These authors contributed equally to this work.

Experimental and Theoretical Demonstrations for the Mechanism behind Enhanced Microbial Electron Transfer by CNT Network

Xian-Wei Liu[1,4]*, Jie-Jie Chen[1]*, Yu-Xi Huang[1], Xue-Fei Sun[2], Guo-Ping Sheng[1], Dao-Bo Li[1], Lu Xiong[1], Yuan-Yuan Zhang[1], Feng Zhao[3] & Han-Qing Yu[1,4]

[1]Department of Chemistry, University of Science & Technology of China, Hefei, 230026, China, [2]School of Environmental Science and Engineering, Shandong University, Jinan, 250100, China, [3]Institute of Urban and Environment, Chinese Academy of Sciences, Xiamen, 361021, China, [4]Collaborative Innovation Center of Suzhou Nano Science and Technology, University of Science & Technology of China, Hefei, 230026, China.

Bioelectrochemical systems (BESs) share the principle of the microbially catalyzed anodic substrate oxidation. Creating an electrode interface to promote extracellular electron transfer from microbes to electrode and understanding such mechanisms are crucial for engineering BESs. In this study, significantly promoted electron transfer and a 10-times increase in current generation in a BES were achieved by the utilization of carbon nanotube (CNT) network, compared with carbon paper. The mechanisms for the enhanced current generation with the CNT network were elucidated with both experimental approach and molecular dynamic simulations. The fabricated CNT network was found to be able to substantially enhance the interaction between the *c*-type cytochromes and solid electron acceptor, indicating that the direct electron transfer from outer-membrane decaheme *c*-type cytochromes to electrode might occur. The results obtained in this study will benefit for the optimized design of new materials to target the outer membrane proteins for enhanced electron exchanges.

Recent efforts have been made on the utilization of dissimilatory metal-reducing bacteria, e.g., *Shewanella* or *Geobacter*, to design bioelectrochemical systems (BESs) for power generation[1], contaminant detoxification[2] and microbial electrosynthesis[3]. A better understanding of the electron transfer mechanisms at microbe/electrode interface is crucial for engineering BES[4–6]. Three distinct extracellular electron transfer pathways, i.e., through cell-surface proteins, mediator compounds (such as flavins), and cellular pili, also named nanowires, have been proposed in BESs. For some bacteria such as *Shewanella*, usually more than one type of extracellular electron transfer pathways are involved[7–9].

Modification of electrode surface at a molecular scale allows an efficient electron transfer between an electrode and a redox protein to develop enzymatic biosensors or biofuel cells[10,11]. Several approaches have been used to facilitate such an electron transfer and accordingly enhance the BES performance, e.g., applying different chemical catalysts, bioactive redox compounds and alkanethiol self-assembled monolayer[12–16]. With excellent electrocatalytic capacity and small size, carbon-based nanomaterials have been recently used to fabricate BES anodes[17–20]. Carbon nanotubes (CNTs)/polyaniline composite was coated onto nickel foams with polytetrafluoroethylene as a binder[18], and such a composite resulted in increased current density. In more recent studies, CNTs and graphene were respectively coated on carbon paper and sponge for improving current generatio[19–21]. However, the mechanisms behind the enhanced current generation at the reported CNT-modified electrodes are unclear yet[21]. Because of the population-level effects of biofilm, secreted mediators, and multiple routines for electron transfer, it is difficult to fractionate the contributions of different mechanisms to current generation and identify the exact reason for the enhanced current generation by the carbon-based nanomaterials.

Therefore, the objective of this study was to elucidate the enhanced electron transfer mechnisms at the bacteria/electrode interface, with CNT network as an example. To achieve this, we chose *Shewanella oneidensis* MR-1 wild type and its mutant strains as model microbes and investigated the interactions between *Shewanella* and CNT network through recoding current at the CNT network electrode with a constant poised potential. In addition, the

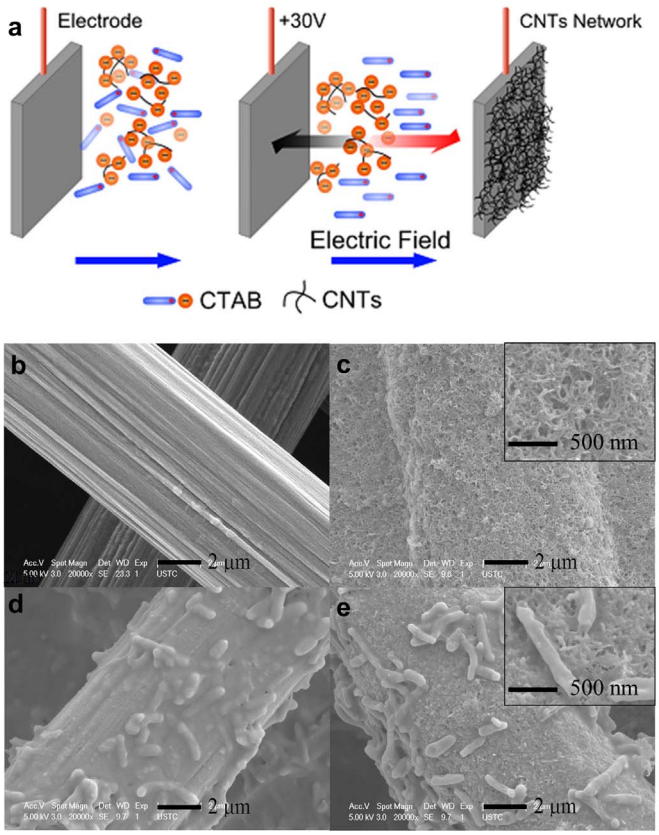

Figure 1 | Schematic of the preparation of the CNT-network-modified electrode (a), SEM images of the carbon paper (b), the CNT network modified-carbon paper (c), biofilms attached on the carbon paper (d), and biofilms attached on the CNT network modified-carbon paper (e).

electron transfer mechanisms at the molecular scale were explored with molecular dynamic simulations. A molecular dynamic model of the porphyrin/CNT conjugates was constructed to test our hypothesis that the porphyrin/CNT proximity might result in the enhanced electron transfer.

Results

Characteristics of the CNT network. To probe the interface processes, the CNT network on a rough carbon paper was constructed with the electrophoretic deposition method as reported previously (Figure 1a)[22]. This method provides a robust coverage of charged particles or molecular clusters on electrode surface. SEM images of the carbon paper taken before and after the modification with CNTs are shown in Figure 1b and c. The graphite fiber surface on the raw carbon paper could be clearly identified with a slick structure, while after the modification, the carbon paper was enwrapped with CNTs. The deposits were relatively homogenous at a larger scale, and nano-sized pores were observed, indicating the formation of hierarchical porous 3D networks.

Raman spectroscopy was used to characterize the structure and topology of the electrode modified with the CNT network. The disorder-induced line near 1320 cm^{-1} showed a significant increase in relative intensity (Figure 2a)[23]. The defective sites on the modified electrode resulted from the oxygen-containing groups, as evidenced by the X-ray photoelectron spectroscopy (XPS) analysis. The O1s photoemission peak was clearly observed on the carbon paper modified by the CNT network, as indicated by an increase in the O1s peak intensity (Figure 2b). The XPS analysis of C1s spectra (Figure 2c and d) shows more information about the surface functional groups on the electrode. An asymmetric peak from sp^2 hybridized carbons centred at 284.5 eV with an extended tail at the higher energy region was generated from the carbon paper, and the same form of the asymmetric peak was used for all other fittings of the sp^2 hybridized graphite-like carbons (Figure 2c). With this asymmetric peak as a reference, the C1s peak of the CNT network was fitted to three Gaussian-Lorentzian shape peaks, which are attributed to C-N or hydroxyls C-OH (286.2 ± 0.1 eV), carbonyls C=O (287.8 ± 0.2 eV), and carboxyls O=C-OH (288.9 ± 0.2 eV) (Figure 2d)[24].

To characterize the electrochemical properties of the CNT network, cyclic voltammetry (CV) and Nyquist plots of impedance measurements for electron transfer probe $Fe(CN)_6^{3-}/^{4-}$ were conducted for the electrode modified with CNT network, with the carbon paper electrode as control. A sharp increase in the redox peak and a great narrowing of the peak-to-peak separation were observed for the CNT-network-modified electrode (Figure 2e), implying its greater electrochemical ability than the raw carbon paper. In addition, the electrochemical active surface areas were calculated from the CV data, 7.3 cm^2 for the CNT network electrode and 2.1 cm^2 for the control electrode (the geometric area of the electrode was 1 cm^2). This result indicates that the CNT network had a higher electrochemical activity towards electron transfer than the control. Such a result was further confirmed by the Nyquist plots of impedance measurements. The semicircular portion at a higher frequency represents the electron-transfer-limited process. The Nyquist plots clearly show that a decrease in the charge-transfer resistance was attributed to the CNT network modified on the carbon paper (Figure 2f).

Enhanced current generation with the CNT network electrode. Interfacial electron collection was monitored with the dose of lactate as carbon source and electron donor. The current density increased to 0.26 A/m^2 with the carbon paper as a control (Figure 3a). However, for the carbon paper coated with the CNT network, the current density drastically increased and reached 2.65 A/m^2. This is a distinctive improvement in the microbial extracellular electron transfer. The current decreased 20 h later, but quickly recovered after the second lactate injection, indicating that the modified electrode was stable. Images of the cells on the carbon paper and the CNT network shown in Figure 1d and e suggest that this method provided a robust coverage of charged particles or molecular clusters on the electrode surface.

The performance of the CNT network as an electrical connection to microbial cells was also evaluated in a microbial fuel cell. The current density of the fuel cell for the CNT anode was 0.29 A/m^2. This value was also substantially higher than that with the carbon paper anode (0.09 A/m^2, Figure 3b).

One reason for the current increase with the CNT electrode might be to the extra attached-growth cells because of the large surface area of the nanotube network. After the experiments, biomass standardized to the attached proteins on the two electrodes was measured, which was 11.4 ± 0.3 μg of proteins for the CNT network electrode and 10.6 ± 0.5 μg of proteins for the carbon paper electrode. Thus, the attached electrode biomass should not be responsible for the increase by 10 times in current at the CNT electrode. *S. oneidensis* is known to produce redox compounds, i.e., flavins, which can act as a mediator between cells and solid electron acceptor. The redox mediators excreted by *S. oneidensis* are usually found at a level of μM or nM. They could accelerate electron transfer and allow catalyzing electron transfer at a lower applied potential[8]. In order to explore the role of flavins as an electron shuttle, the CV analysis was performed (Figure 4a). The redox peak current with the CNT network was in the same order as that with the carbon paper. Obviously, this slight improvement could not be responsible for the increase in microbial current by 10 times, especially at a low flavin concentration.

Cytochromes *MtrC* and *OmcA* are located on the extracellular face of the outer membrane, and can be directly involved in electron

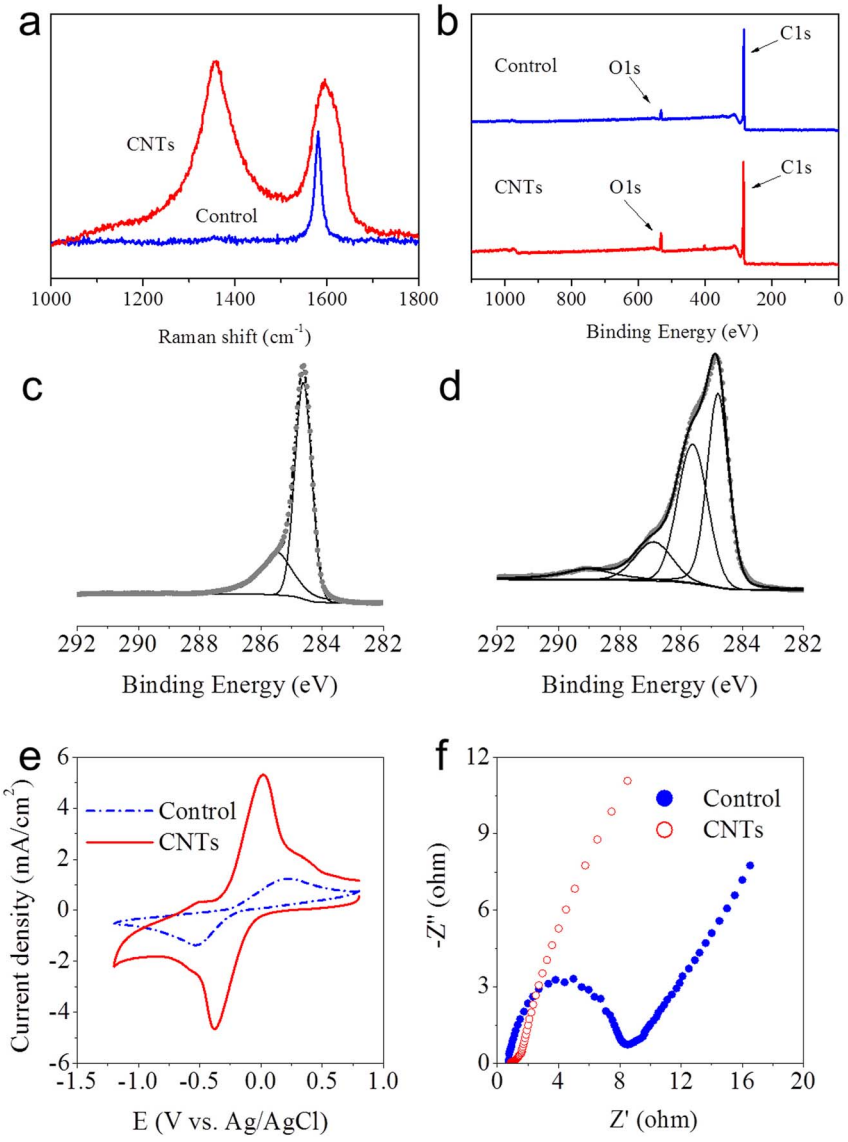

Figure 2 | Raman spectra (a) and XPS survey (b) of the electrodes with the carbon paper and the CNT-network-modified carbon paper; XPS C1s spectra of the carbon paper (c), the CNT-network modified-carbon paper (d), CVs of 0.5 mM $[Fe(CN)_6]^{3-/4-}$ in 0.1 M KCl (pH 7.0) at a scan rate of 100 mV/s (e), Nyquist plots of 10 mM $[Fe(CN)_6]^{3-/4-}$ in 0.1 M KCl from 100 KHz to 0.1 Hz at an ac amplitude of 5 mV under open-circuit potential conditions (f).

transfer to an extracellular acceptor[25]. To elucidate whether the direct connection between CNTs and c-type cytochromes is responsible for the promoted electron transfer at the interface, a *S. oneidensis* MR-1 mutant deleting *MtrC* and *OmcA* was tested with electrochemical methods (Figure 4b). The current density generated by the mutant Δ*OmcA/MtrC* for the CNT network (0.11 A/m^2) was higher than that for the carbon paper (0.01 A/m^2). Deletion of specific cytochromes significantly decreased the current but did not affect its attachment to the electrode surface (data not shown), indicating that both *MtrC* and *OmcA* played a key role in the electron transfer at cells and electrode interface. To get a further insight into the interactions between the CNT and the *c*-type cytochromes, CV of *S. oneidensis* MR-1 biofilm in a lactate-free medium under anaerobic conditions was analyzed. In order to deplete internal electron donor pools and facilitate attachment, *S. oneidensis* cells in all the systems were incubated with electrodes poised at oxidizing potentials prior to analysis. For *S. oneidensis* MR-1 on the CNTs, a clear redox peak was observed with a midpoint potential of −0.08 V vs Ag/AgCl (Figure S3). The catalytic current of *S. oneidensis* MR-1 biofilm on the CNT network was higher than that on the glassy carbon electrode. This observation was in agreement with the results that the CNTs enhanced the microbial electron transfer.

Molecular dynamic simulations. To find out the exact reasons for the accelerated electron transfer rate from the outer membrane *c*-type cytochromes of *S. oneidensis* MR-1 to the electrode by the CNT, molecular dynamic simulations were used to explore the mechanisms for the direct electron transfer from iron(II) in the reduced *c*-type cytochromes to the CNT network at a molecular level. Porphyrin iron is the centre structure of *c*-type cytochromes, which plays an important role in the redox process (Figure 5a). The ring of porphyrin iron in the initial structure is almost in a plane along *x* direction (YZ-plane) (Figure S4). The porphrin ring in models is distorted to form specific molecular configuration with lattice relaxation in its interactions with carbon-based materials (Figure 5b–e). The alkyl and carboxyl groups in the porphyrin ring are bended, surrounding the CNTs with the porphyrin ring distorted, as shown in Figure 5d and 5e. The bent radian of porphyrin iron

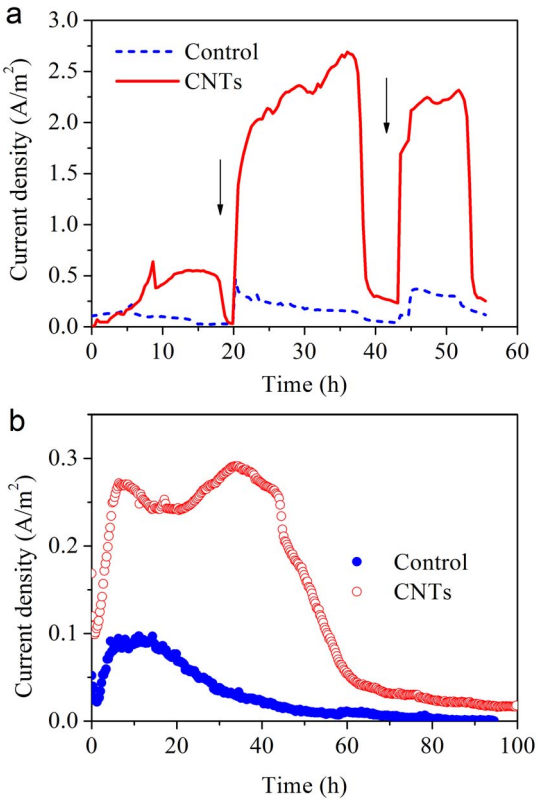

Figure 3 | Microbial current generation of the three-electrode system with the wild-type S. *oneidensis* MR-1 using the CNT-network as the working electrode (a); performance of the MFCs using the CNT-network as the anode (b). Arrow indicates lactate is injected.

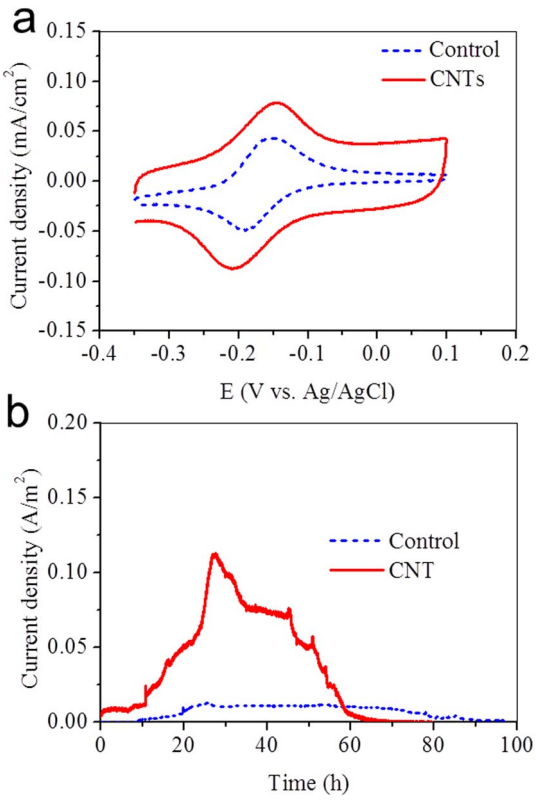

Figure 4 | CVs of 5 μM flavin in 0.1 M Na_2SO_4 solution at the carbon paper and the CNT-network modified-carbon paper (a), Microbial current generation of the three-electrode system with Δ*OmcA*/*MtrC* mutant (b).

molecules is almost the same as the curvature of CNTs. The geometry parameters of the distorted porphyrin rings obtained from the analysis of simulations are summarized Table S1. The shift in the bond angles of N1-Fe-N3 and N2-Fe-N4 enables the active centre of Fe^{2+} in the electron donor to approach close to the electron acceptor, such as carbon materials, and reduce the distance for electron transfer. The shortest distance between Fe^{2+} of porphyrin iron and carbon atom of electron acceptors in the cytochromes-graphite system is about 17 Å, while the corresponding value in the cytochromes-CNT system is drastically decreased to 4Å only. The shortest cytochromes-CNT distance for electron transfer indicates that the CNT could accelerate the electron transfer at the microbes/electrode interface.

The promotion of microbial electron transfer by the nanotubes is further confirmed with a thermodynamic analysis on the interactions between *c*-type cytochromes and carbon-based materials. The interaction energy (ΔE_{inter}) is defined as total energy change in the process that the structure of the redox center of cytochrome, porphyrin iron, approaches to the surface of carbon materials with one-electron transfer. ΔE_{inter} of these systems is given as follows:

$$\Delta E_{inter} = E_{total}\left[Cyt\left(Fe^{3+}\right)\right] - E_{total}\left[Cyt\left(Fe^{2+}\right)\right] \quad (1)$$

where $E_{total}[Cyt\ (Fe^{3+})]$ is the total energy of cytochrome-graphite or cytochrome-CNT in its oxidized state, and $E_{total}[Cyt\ (Fe^{2+})]$ is the total energy of that in its reduced state. The values of the total energy in Table 1 were obtained from the molecular dynamic simulations with the Discover module.

The interaction energies of the two systems are listed in Table 1. The negative value of ΔE_{inter} indicates that the system becomes more stable after releasing one electron. Moreover, ΔE_{inter} of the cytochrome-CNT system with a more negative value than that of the cytochrome-graphite system implies that that the CNT network facilitates the acceptance of electrons from Fe^{2+} in the reduced *c*-type cytochromes. This result is in agreement with the geometry analysis results above. To exclude the the effect of CNT diameter on the electron transfer, the electron transfer systems with CNTs at three different diameters of 5, 15, and 25 nm were also calculated (Figure S5 and Table S2). The results are in agreement with that of the system with small-diameter CNTs.

Discussion

In this work, a CNT network-based electrode interface was fabricated to promote microbial extracellular electron transfer from microbes to electrode and the mechanisms for such an enhancement were elucidated by experimental and computational approaches.

Nanosized materials have been used to increase current generation in microbial fuel cells[14,20,21]. However in the previous reports, the mechanisms responsible for this improvement have not been investigated and some were attributed to a high biomass colonization on these electrodes[16]. As for *S. oneidensis* MR-1, the outer membrane c-type cytochrome exhibited a high affinity to nanosized metal oxides[26]. This interaction not only enabled bacteria insert electrons into the metal oxides[25,27], but also enhanced the bacteria/solid interfacial and interspecies electron transfers[28,29]. However, in a BES how the electron transfer could be modulated rather than only a high biomass colonization by CNTs is unknown yet.

Figure 5f and g shows the electron transfer pathway, which is proposed on the basis of our experimental results and previous reports. Cytochromes *MtrC* and *OmcA* are located on the extracellular face of the outer membrane, and can be directly involved in electron transfer to an extracellular solid acceptor, such as Fe(III) minerals[4], or to extracellular electron shuttles[8]. Because of the size

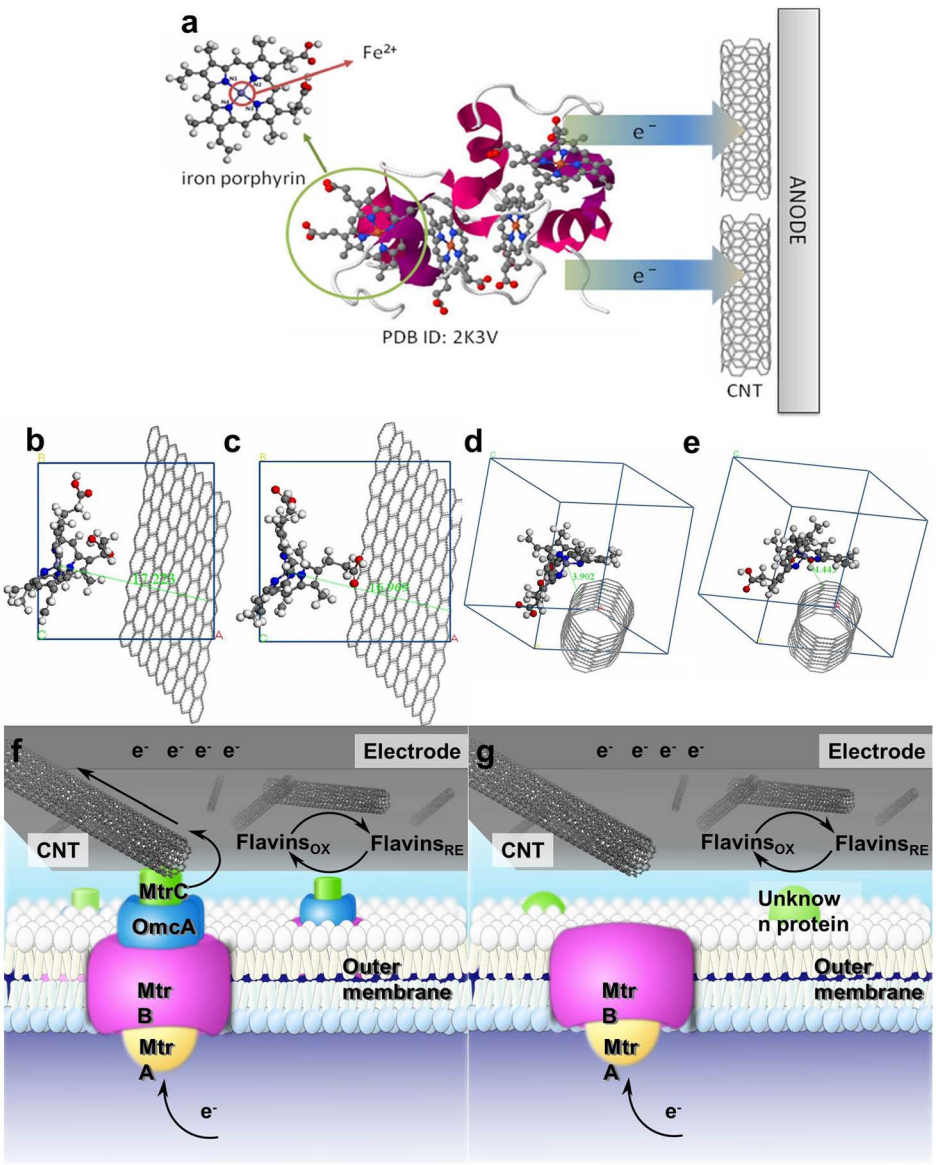

Figure 5 | Stereoview of *Shewanella*'s small tetraheme cytochrome using the same representation as depicted in Leys et al[38].: the cytochrome backbone is shown in violet, the porphyrin rings in gray, and the iron atoms in orange (a). cytochromes-graphite (Fe^{2+}) a = 17.0668 Å, b = 17.0700 Å, c = 17.0636 Å, α = β = γ = 90 (b); cytochromes-graphite (Fe^{3+}) a = 17.0668 Å, b = 17.0700 Å, c = 17.0636 Å, α = β = γ = 90° (c); cytochromes-CNT (Fe^{2+}) a = b = c = 17.1123 Å, α = β = γ = 90° (d); and cytochromes-CNT (Fe^{3+}) a = b = c = 17.1123 Å, α = β = γ = 90° (e). Schematic illustration of electron transfer at the interface of CNTs and the outer membrane of the wild-type *S. oneidensis* MR-1 (f); and the outer membrane of Δ*OmcA/MtrC* mutant (g).

effect of CNTs, the direct communication between active site of cytochromes and CNTs is feasible. In addition, the CNT network is rich in redox functional groups, as evidenced by XPS (Figure 2), which are also useful to accelerate electron transfer at the bacteria/electrode interface (Figure 5f)[30]. Δ*OmcA/MtrC* mutant was severely impaired in the sustained electron transfer rate, but it could attach to electrodes in a similar manner[31]. When the Δ*OmcA/MtrC* mutant was used, the current with a small background level resulted from the interaction between the CNT network and unknown proteins (Figure 5g). In addition, molecular dynamic simulations further

Table 1 | Total energy (E_{total}) and interaction energy (ΔE_{inter}) of electron transfer from porphyrin iron to carbon materials at ambient temperatures

system	E_{total} (mean) (kcal/mol)	std. dev.[a]	ΔE_{inter} (kcal/mol)
cytochrome-graphite (Fe^{2+})	2889.984	13.504	−4.835
cytochrome-graphite (Fe^{3+})	2885.149	15.693	
cytochrome-CNT (Fe^{2+})	4615.448	15.595	−8.367
cytochrome-CNT (Fe^{3+})	4607.081	15.051	

[a]std. dev.: standard deviation.

confirm the experimental results and reveal that the interaction between the CNT network and *c*-type cytochromes is one of the main mechanisms responsible for the enhanced microbial electron transfer, which is associated with the distorted porphyrin ring, short distance of electron transfer and more negative interaction energy.

In summary, we have achieved the enhanced extracellular electron transfer from bacteria to electrode through CNT network, and presented clear evidence for the role of the CNT network to bridge cell cytochromes and electron acceptor for such an enhancement using both experimental and computational approaches. The results obtained in this study will benefit for designing new materials to target the outer membrane protein for enhanced electron exchanges between cells and electrode.

Methods

Fabrication of the CNT network. CNTs with an average diameter of 20–40 nm and a length of 5–15 μm were purchased from Nanoport Co., Shenzhen, China. The CNTs were purified and functionalized by sonication in a 1 : 3 mixture of 70% nitric acid and 97% sulfuric acid for 4 h, followed by precipitation and rinsing with water. All other chemicals were of analytical grade and used without further purification. CNTs were solubilized by mixing 10 mg of CNTs with 168.5 mg of cetyltrimethylammonium bromide (CTAB) in 25-mL tetrahydrofuran and sonicating the mixture for 30 min. After the sample was subjected to centrifugation for 15 min at 10000 rpm, the residue was re-suspended in tetrahydrofuran. This sonication/centrifugation process was repeated for 3–4 cycles to remove excess CTAB. Two carbon papers (3×3 cm^2, 190 μm thickness, Toray Co., Japan) were kept ~5 mm apart in a cell containing a CNT suspension in tetrahydrofuran. A dc voltage of ~30 V was applied for 10 min. The carbon paper was then removed from the solution and rinsed with water to obtain a CNT network-modified electrode.

Cell cultures. The wild type *S. oneidensis* MR-1 and its mutant strains, kindly provided by Prof. K. H. Nealson at the University of Southern California[32], were grown from a frozen stock, first aerobically in 100-ml Luria-Bertani broth, a solution of 10 g/L tryptone, 5 g/L NaCl, and 5 g/L yeast extract, at 30°C for 12 h. Subsequently, the culture was incubated in a mineral medium for electricity generation, which contained (per liter) 10 mM Hepes, 0.46 g of NH_4Cl, 0.225 g of K_2HPO_4, 0.225 g of KH_2PO_4, 0.117 g of $MgSO_4 \cdot 7H_2O$, and 0.225 g of $(NH_4)_2SO_4$. Prior to autoclaving, 10 ml of a mineral mix (containing in per liter 1.5 g of nitrilotriacetic acid, 0.1 g of $MnCl_2 \cdot 4H_2O$, 0.3 g of $FeSO_4 \cdot 7H_2O$, 0.17 g of $CoCl_2 \cdot 6H_2O$, 0.1 g of $ZnCl_2$, 0.04 g of $CuSO_4 \cdot 5H_2O$, 0.005 g of $AlK(SO_4)_2 \cdot 12H_2O$, 0.005 g of H_3BO_3, 0.09 g of Na_2MoO_4, 0.12 g of $NiCl_2$, 0.02 g of $NaWO_4 \cdot 2H_2O$, and 0.10 g of Na_2SeO_4) was added. All vitamins were eliminated.

Microbial current measurements. A single-chamber three-electrode system was used, in which a Ag/AgCl (KCl sat.) and a Pt wire were respectively used as reference electrode and counter electrode. The CNT network modified-carbon paper was used as the anode, while the raw carbon paper was employed for the control experiment (Figure S1). The freshly prepared cell suspension was inoculated into the reactor at a constant voltage of 0.1 V (vs. Ag/AgCl, 25°C, pH 7.0) over 12 h to facilitate microbial attachment to the electrode surface[31]. Then, 1 mL of concentrated lactate solution was injected to the chamber to make a concentration 10 mM.

Molecular dynamic simulations. Amorphous model of reactants was constructed at 298 K with porphyrin iron(II) and (5, 5) CNT with a diameter of 6.78 Å and length of 23.18 Å, and the products were composed of porphyrin iron(III) and the CNT as the same as the reactant model. In order to explain the performance of the CNT for electron transfer, the graphite layer was introduced as another carbon material into the amorphous models in comparison with the CNT. All the molecular simulations were carried out using the Discover module of Materials Studio package, automatically applying appropriate options at each stage of processing. This module incorporates a range of well-validated forcefields for dynamic simulations, minimization, and conformational searches, to predict the structure, energetics, and properties of organic, inorganic, organometallic, and biological systems[33]. A detailed description is given in Supporting Information. Model simulations were executed with the energy minimization step using the smart minimize method, which is a combination of the steepest descent, conjugated gradient, and Newton methods in a cascade. In this case, the convergence levels were set to 0.01, 0.01, and 0.1 kcal/mol·Å, respectively. The nonbond interactions (electrostatic and van der Waals) were calculated with the Ewald summation method[34] with an accuracy of 0.01 kcal/mol, which has been proven to be appropriate for calculation in many systems[35,36]. With energy minimized amorphous cells of reactants and products, MD simulations were performed under NVT ensemble using a time step of 1.0 fs for equilibrating the models. The dynamics were modified to allow the system to exchange heat with the environment at a controlled temperature of 298 K. The consistent valence force field (CVFF) was used for reactants and products[37]. The Andersen algorithm set to a collision ratio of 1.0 was used to control the temperature of each model. The main objective of equilibration is to bring the electron transfer system to the most probable configuration consistent with the target temperature.

1. Logan, B. E. & Rabaey, K. Conversion of wastes into bioelectricity and chemicals by using microbial electrochemical technologies. *Science* **337**, 686–690 (2012).
2. Mu, Y., Rozendal, R. A., Rabaey, K. & Keller, J. R. Nitrobenzene removal in bioelectrochemical systems. *Environ. Sci. Technol.* **43**, 8690–8695 (2009).
3. Rabaey, K. & Rozendal, R. A. Microbial electrosynthesis - revisiting the electrical route for microbial production. *Nature Rev. Microbiol.* **8**, 706–716 (2010).
4. Hartshorne, R. S. *et al.* Characterization of an electron conduit between bacteria and the extracellular environment. *Proc. Nat. Acad. Sci. U. S. A.* **106**, 22169–22174 (2009).
5. Holmes, D. E. *et al.* Microarray and genetic analysis of electron transfer to electrodes in Geobacter sulfurreducens. *Environ. Microbiol.* **8**, 1805–1815 (2006).
6. Wu, X. *et al.* A Role for Microbial palladium nanoparticles in extracellular electron transfer. *Angew. Chem. Int. Ed.* **50**, 427–430 (2011).
7. El-Naggar, M. Y. *et al.* Electrical transport along bacterial nanowires from *Shewanella oneidensis* MR-1. *Proc. Nat. Acad. Sci. U. S. A.* **107**, 18127–18131 (2010).
8. Marsili, E. *et al. Shewanella* secretes flavins that mediate extracellular electron transfer. *Proc. Nat. Acad. Sci. U. S. A.* **105**, 3968–3973 (2008).
9. Reguera, G. *et al.* Extracellular electron transfer via microbial nanowires. *Nature* **435**, 1098–1101 (2005).
10. Gooding, J. J. *et al.* Protein electrochemistry using aligned carbon nanotube arrays. *J. Am. Chem. Soc.* **125**, 9006–9007 (2003).
11. Liu, X.-W., Li, W.-W. & Yu, H.-Q. Cathodic catalysts in bioelectrochemical systems for energy recovery from wastewater. *Chem. Soc. Rev.* doi: 10.1039/c3cs60130g (2013).
12. Chen, S. *et al.* Electrospun and solution blown three-dimensional carbon fiber nonwovens for application as electrodes in microbial fuel cells. *Energy Environ. Sci.* **4**, 1417–1421 (2011).
13. Liu, X.-W. *et al.* Phenothiazine derivative-accelerated microbial extracellular electron transfer in bioelectrochemical system. *Sci. Rep.* **3**, 1616 (2013).
14. Qiao, Y. *et al.* Nanostructured polyaniline/titanium dioxide composite anode for microbial fuel cells. *ACS Nano* **2**, 113–119 (2007).
15. Rosenbaum, M., Zhao, F., Schroder, U. & Scholz, F. Interfacing electrocatalysis and biocatalysis with tungsten carbide: A high-performance, noble-metal-free microbial fuel cell. *Angew. Chem. Int. Ed.* **45**, 6658–6661 (2006).
16. Yong, Y.-C., Dong, X.-C., Chan-Park, M. B., Song, H. & Chen, P. Macroporous and monolithic anode based on polyaniline hybridized three-dimensional graphene for high-performance microbial fuel cells. *ACS Nano* **6**, 2394–2400 (2012).
17. Peng, L., You, S.-J. & Wang, J.-Y. Carbon nanotubes as electrode modifier promoting direct electron transfer from *Shewanella oneidensis*. *Biosensors Bioelectron.* **25**, 1248–1251 (2010).
18. Qiao, Y., Li, C. M., Bao, S. J. & Bao, Q. L. Carbon nanotube/polyaniline composite as anode material for microbial fuel cells. *J. Power Sources* **170**, 79–84 (2007).
19. Sun, J.-J., Zhao, H.-Z., Yang, Q.-Z., Song, J. & Xue, A. A novel layer-by-layer self-assembled carbon nanotube-based anode: Preparation, characterization, and application in microbial fuel cell. *Electrochim. Acta* **55**, 3041–3047 (2010).
20. Xie, X. *et al.* Three-dimensional carbon nanotube−textile anode for high-performance microbial fuel cells. *Nano Lett.* **11**, 291–296 (2010).
21. Huang, Y.-X. *et al.* Graphene oxide nanoribbons greatly enhance extracellular electron transfer in bio-electrochemical systems. *Chem. Comm.* **47**, 5795–5797 (2011).
22. Brown, P. & Kamat, P. V. Quantum dot solar cells. electrophoretic deposition of CdSe−C_{60} composite films and capture of photogenerated electrons with nC_{60} custer shell. *J. Am. Chem. Soc.* **130**, 8890–8891 (2008).
23. Ferrari, A. C. & Robertson, J. Interpretation of Raman spectra of disordered and amorphous carbon. *Phys. Rev. B* **61**, 14095 (2000).
24. Lee, S. W., Kim, B.-S., Chen, S., Shao-Horn, Y. & Hammond, P. T. Layer-by-layer assembly of all carbon nanotube ultrathin films for electrochemical applications. *J. Am. Chem. Soc.* **131**, 671–679 (2008).
25. White, G. F. *et al.* Rapid electron exchange between surface-exposed bacterial cytochromes and Fe(III) minerals. *Proc. Nat. Acad. Sci. U. S. A.* doi: 10.1073/pnas.1220074110 (2013).
26. Xiong, Y. *et al.* High-affinity binding and direct electron transfer to solid metals by the *Shewanella oneidensis* MR-1 outer membrane c-type cytochrome OmcA. *J. Am. Chem. Soc.* **128**, 13978–13979 (2006).
27. Yuan, S.-J. *et al.* A photometric high-throughput method for identification of electrochemically active bacteria using a WO_3 nanocluster probe. *Sci. Rep.* **3**, 1315 (2013).
28. Kato, S., Hashimoto, K. & Watanabe, K. Microbial interspecies electron transfer via electric currents through conductive minerals. *Proc. Nat. Acad. Sci. U. S. A.* **109**, 10042–10046 (2012).
29. Nakamura, R., Kai, F., Okamoto, A., Newton, G. J. & Hashimoto, K. Self-constructed electrically conductive bacterial networks. *Angew. Chem. Int. Ed.* **48**, 508–511 (2009).
30. Fredrickson, J. K. *et al.* Towards environmental systems biology of Shewanella. *Nat. Rev. Micro.* **6**, 592–603 (2008).
31. Baron, D., LaBelle, E., Coursolle, D., Gralnick, J. A. & Bond, D. R. Electrochemical measurement of electron transfer kinetics by *Shewanella oneidensis* MR-1. *J. Biol. Chem.* **284**, 28865–28873 (2009).

32. Bretschger, O. *et al.* Current production and metal oxide reduction by *Shewanella oneidensis* MR-1 wild type and mutants. *Appl. Environ. Microbiol.* **73**, 7003–7012 (2007).
33. Lombardo, G. M., Pappalardo, G. C., Costantino, F., Costantino, U. & Sisani, M. Thermal effects on mixed metal (Zn/Al) layered double hydroxides: direct modeling of the X-ray powder diffraction line shape through molecular dynamics simulations. *Chem. Mater.* **20**, 5585–5592 (2008).
34. Essmann, U. *et al.* A A smooth particle mesh Ewald method. *J. Chem. Phys.* **103**, 8577–8593 (1995).
35. Chen, Z.-M., Çağin, T. & Goddard, W. Fast Ewald sums for general van der Waals potentials. *J. Comput. Chem.* **18**, 1365–1370 (1997).
36. Scocchi, G., Posocco, P., Fermeglia, M. & Pricl, S. Polymer−Clay Polymer-clay nanocomposites: a multiscale molecular modeling approach. *J. Phys. Chem. B* **111**, 2143–2151 (2007).
37. Dauber-Osguthorpe, P. *et al.* Structure and energetics of ligand binding to proteins: *Escherichia coli* dihydrofolate reductase-trimethoprim, a drug-receptor system. *Proteins Struct. Funct. Genet.* **4**, 31–47 (1988).
38. Leys, D. *et al.* Crystal structures at atomic resolution reveal the novel concept of "electron-harvesting" as a role for the small tetraheme cytochrome c. *J. Biol. Chem.* **277**, 35703–35711 (2002).

Acknowledgments

This work is partially supported by the National Natural Science Foundation of China (51129803), the Program for Changjiang Scholars and Innovative Research Team in University of the Ministry of Education of China, and the National Synchrotron Radiation Laboratory, Hefei, China. Prof. K.H. Nealson at the University of Southern California is acknowledged for his kind provision of *S. oneidensis* MR-1 and its mutants.

Author contributions

X.W.L., Y.X.H., X.F.S., G.P.S. and H.Q.Y. designed the experiments; J.J.C. conducted the DFT calculations and molecular dynamics simulations; X.W.L., Y.X.H., X.F.S., D.B.L., X.L. and Y.Y.Z. conducted the experiments; X.W.L., G.P.S., F.Z. and H.Q.Y. contributed to the planning and coordination of the project; X.W.L., G.P.S., F.Z., J.J.C. and H.Q.Y. wrote and edited the manuscript. All authors contributed to discussions about the results and the manuscript.

Additional information

Supplementary information accompanies this paper at http://www.nature.com/scientificreports

Competing financial interests: The authors declare no competing financial interests.

How to cite this article: Liu, X.-W. *et al.* Experimental and Theoretical Demonstrations for the Mechanism behind Enhanced Microbial Electron Transfer by CNT Network. *Sci. Rep.* **4**, 3732; DOI:10.1038/srep03732 (2014).